LANGMUIR

Active Brownian Motion with Orientation-Dependent Motility: Theory and Experiments

Alexander R. Sprenger, Miguel Angel Fernandez-Rodriguez, Laura Alvarez, Lucio Isa,* Raphael Wittkowski,* and Hartmut Löwen

Cite This: *Langmuir* 2020, 36, 7066−7073

Read Online

ACCESS | Metrics & More | Article Recommendations | Supporting Information

ABSTRACT: Combining experiments on active colloids, whose propulsion velocity can be controlled via a feedback loop, and the theory of active Brownian motion, we explore the dynamics of an overdamped active particle with a motility that depends explicitly on the particle orientation. In this case, the active particle moves faster when oriented along one direction and slower when oriented along another, leading to anisotropic translational dynamics which is coupled to the particle's rotational diffusion. We propose a basic model of active Brownian motion for orientation-dependent motility. On the basis of this model, we obtain analytical results for the mean trajectories, averaged over the Brownian noise for various initial configurations, and for the mean-square displacements including their non-Gaussian behavior. The theoretical results are found to be in good agreement with the experimental data. Orientation-dependent motility is found to induce significant anisotropy in the particle displacement, mean-square displacement, and non-Gaussian parameter even in the long-time limit. Our findings establish a methodology for engineering complex anisotropic motilities of active Brownian particles, with a potential impact in the study of the swimming behavior of microorganisms subjected to anisotropic driving fields.
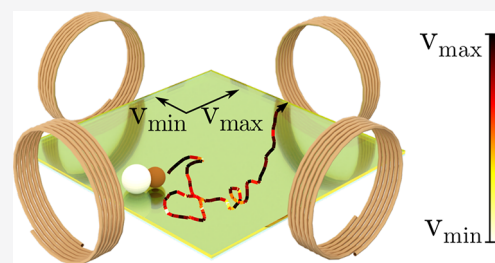
INTRODUCTION

Active Brownian particles, the synthetic analogues of biological microswimmers such as bacteria and protozoa, have the ability to self-propel at low Reynolds numbers via the conversion of energy available in their surroundings into directed motion by exploiting intrinsic asymmetries in their shape and material properties.[1,2] Their motion arises from the interplay between thermal fluctuations and propulsion, which renders active colloids an excellent model system for studying far-from-equilibrium physical phenomena,[3−5] also featured in their biological counterparts. The basic model for describing the trajectories of a self-propelling colloid, called active Brownian motion, couples a constant velocity v along the particle's asymmetry direction with its rotational diffusivity D_R, which constantly randomizes the propulsion direction with a characteristic time scale $\tau_R = 1/D_R$. In this model, the particle displacements result from propulsion combined with stochastic translational and rotational noise. The propensity for straight paths is defined by the persistence length of the trajectory, $L_P = v/D_R$. To date, various propulsion mechanisms have been realized for active colloids. Among them are self-propulsion induced by chemical reactions,[6−8] illumination,[9−14] or ultrasound[15] and actuation by magnetic[16−19] or electric[20,21] fields. Regardless of the origin of propulsion, the scenario defined by active Brownian motion[1] was verified in experiments for a range of artificial microswimmers.[22−24]

Despite the success of ordinary active Brownian motion, the complexity of some behaviors found in biological and artificial microswimmers implies the urge to extend our experimental and theoretical models, in particular, to include complex spatio-temporal dependencies of propulsion velocity as well as translational and rotational noise. These situations are frequently encountered for systems where the external stimulus governing the motility is inhomogeneous.[25−32] Recently, motility landscapes, where the particle propulsion speed depends on spatial coordinates, time, or a combination of both,[33−36] have been experimentally realized[25,31,37−41] and numerically modeled.[31,42−49] However, with rare recent exceptions aside,[50] the orientational analogue to a position-dependent motility landscape, which is an orientation-dependent motility, remains unexplored for systems of noninteracting anisotropic active particles.

In this article, we experimentally and theoretically study active dumbbells with an orientation-dependent motility. This system offers a basic setup for anisotropic actuation in which the particle's propulsion speed is modulated according to its orientation, which is constantly randomized by rotational

diffusion, thus introducing anisotropy into the particle dynamics. In our experiments, we use active dumbbell-shaped colloids composed of a polystyrene and a magnetic silica particle assembled via sequential capillary assembly[51] and self-propelling on a planar substrate via alternating electric fields.[52,53] The particle's position and orientation are tracked in real time and used as the input for a feedback loop that updates the particle velocity with full programmability.[54] These results are used to verify the basic theoretical model for active Brownian motion with an orientation-dependent velocity, which we propose and establish here. We obtain analytical results for mean trajectories averaged over the Brownian noise for various initial configurations and arbitrary angular dependencies of the velocity. We further calculate the corresponding mean-square displacements, including their anisotropic non-Gaussian behavior, and characterize the anisotropy as a function of time. We find that the theoretical calculations are in good agreement with the experimental data. The results of this work shed new light on anisotropically active Brownian particles, inspiring both a better understanding of the behavior exhibited by motile micro-organisms when subjected to inhomogeneous or anisotropic driving fields[55] and new design ideas for smarter synthetic microswimmers.

■ MATERIALS AND METHODS

Theoretical Description. In our theoretical model, we consider a single overdamped active Brownian particle in two spatial dimensions. The state of this particle is fully described by the center-of-mass position $\mathbf{r}(t)$ and the angle of orientation $\phi(t)$, which denotes the angle between the orientation vector $\hat{\mathbf{u}} = (\cos\phi, \sin\phi)$ and the positive x axis, at the corresponding time t. The centerpiece of our model is an arbitrary orientation-dependent motility $\mathbf{v}(\phi)$. Without a loss of generality, we represent the propulsion velocity $\mathbf{v}(\phi)$ as a Fourier series

$$\mathbf{v}(\phi) = \bar{v} \sum_{k=-\infty}^{\infty} \mathbf{c}_k \exp(ik\phi) \qquad (1)$$

where $\bar{v}$ denotes a reference velocity, $\mathbf{c}_k$ is the Fourier coefficient vector of mode k, and i denotes the imaginary number. For a given propulsion velocity $\mathbf{v}(\phi)$, these Fourier coefficients can be calculated as $\mathbf{c}_k = \int_{-\pi}^{\pi}(\mathbf{v}(\phi)/(2\pi\bar{v})) \exp(-ik\phi)\, d\phi$. The overdamped Brownian dynamics of the particle is described by the coupled Langevin equations for orientation-dependent motility

$$\dot{\mathbf{r}}(t) = \mathbf{v}(\phi(t)) + \sqrt{2D_T}\,\boldsymbol{\xi}(t) \qquad (2)$$

$$\dot{\phi}(t) = \sqrt{2D_R}\,\eta(t) \qquad (3)$$

where D_T and D_R are the translational and rotational short-time diffusion coefficients of the particle, respectively. To take translational and rotational diffusion into account, the Langevin equations contain independent Gaussian white noise terms $\boldsymbol{\xi}(t)$ and $\eta(t)$, with zero means, $\langle\boldsymbol{\xi}(t)\rangle = 0$ and $\langle\eta(t)\rangle = 0$, and delta-correlated variances, $\langle\xi_i(t_1)\xi_j(t_2)\rangle = \delta_{ij}\delta(t_1 - t_2)$ and $\langle\eta(t_1)\eta(t_2)\rangle = \delta(t_1 - t_2)$, where $i, j \in \{x, y\}$. The brackets $\langle\cdots\rangle$ denote the noise average, and δ_{ij} is the Kronecker delta.

To keep the model initially as general as possible, we prescribe the self-propulsion by a vector function $\mathbf{v}(\phi)$. Later, we will focus on special motility scenarios and proceed to the less general factorization $v_0(\phi)\,\hat{\mathbf{u}}(\phi)$ that is typically assumed in the literature.[1] The special case of isotropic self-propulsion corresponds to the form $v_0\hat{\mathbf{u}}(\phi)$ with a constant speed v_0. It is associated with the only nonzero Fourier coefficient vectors $\mathbf{c}_1 = (1, -i)/2$ and $\mathbf{c}_{-1} = (1, i)/2$. In the following sections, we neglect mode $k = 0$ in eq 1, which would describe a trivial constant drift.

Fabrication of Active Magnetic Dumbbells. Active magnetic dumbbells composed of a 2.0-μm-diameter polysterene (PS) and a 1.7-μm-diameter magnetic silica (SiO$_2$-mag) particle (Microparticles

GmbH) were fabricated using the sequential capillarity-assisted particle assembly (sCAPA) technique as described in previous work.[51] First, a 40 μL water droplet (Milli-Q) with 0.1 mM sodium dodecyl sulfate (SDS, 99.0%, Sigma-Aldrich), 0.01 wt % of surfactant Triton X-45 (Sigma), and 0.5 wt % PS particles was deposited and dragged at a controlled speed over a polydimethylsiloxane (PDMS) template with rectangular traps of 2.2 μm × 1.1 μm lateral dimensions and 0.5 μm depth, fabricated by conventional photolithography. This deposition step resulted in one PS particle deposited per trap, leaving space for a second particle. The process was then repeated with a dispersion of SiO$_2$-mag particles. Individual SiO$_2$-mag particles were deposited inside the traps in close contact with the PS particles forming dumbbells. Next, the dumbbells were sintered in the traps by heating the template to 85 °C for 25 min. Finally, the dumbbells were harvested by freezing a droplet of a 10 μM KCl (Fluka) aqueous solution over the traps and lifting it from the template. The thawed droplet containing the dumbbells was used to fill the experimental cell as described below.

Cell Preparation and Active Motion Control. Transparent electrodes were fabricated from 22 mm × 22 mm glass slides (85−115 μm thick, Menzel Gläser, Germany) coated via e-beam metal evaporation with 3 nm of Cr and 10 nm of Au (Evatec BAK501 LL, Switzerland), followed by a top layer of 10 nm of SiO$_2$ (STS Multiplex CVD, U.K.) deposited by plasma-enhanced chemical vapor deposition. A 7.4 μL droplet of the dumbbell suspension was placed on the bottom electrode inside a 0.12-mm-thick sealing spacer with a 9 mm circular opening (Grace Bio-Laboratories SecureSeal, U.S.).

After sealing the cell with the top electrode, both electrodes were connected to a signal generator (National Instruments Agilent 3352X, U.S.) to apply an ac electric field with a fixed frequency of 1 kHz and varying peak-to-peak voltage $V_{PP}(t)$ of between 1 and 10 V, depending on the dumbbell orientation. The particles are propelled thanks to unbalanced electrohydrodynamic (EHD) flows on each side of the dumbbell, with the SiO$_2$-mag lobe leading the motion. The propulsion velocity is proportional to V_{PP}^2.[52,53]

We furthermore imposed a fixed rotational diffusivity $D_R = 0.25$ rad^2/s for the dumbbells in all experiments, as described in a previous work.[54] In brief, we applied external magnetic fields via two pairs of independent Helmholtz coils to align the magnetic moment of the SiO$_2$-mag particle. The angle $\phi(t)$ of the applied magnetic field is randomly varied in time according to the relation $\phi(t + \Delta t) = \phi(t) + \sqrt{2D_R\Delta t}\,\eta(t)$, where in the experiments $\Delta t = 1$ ms and $\eta(t)$ is defined as above.

Imaging and Feedback Loop. The dumbbells were imaged in transmission mode with a home-built bright-field microscope. Image sequences were taken with a sCMOS camera (Andor Zyla) with a 1024 pixels × 1024 pixels field of view and a 50× objective (Thorlabs). The center of mass $\mathbf{r}(t)$ and the angle $\phi(t)$ of the dumbbells with respect to the x axis were tracked in real time using customized software written in Labview and Matlab. The detected orientation of the dumbbell is symmetric with respect to π, being 0 or π when it is perfectly aligned with the x axis. After the experiments, we postprocessed the acquired images to identify both lobes of the dumbbell and convert the angles to the interval from 0 to 2π. The velocity of the dumbbell was varied as a function of its orientation by changing the applied peak-to-peak voltage V_{PP} according to

$$V_{PP}(t) = (V_{PP}^{max} - V_{PP}^{min})\sin^2(n\phi(t)) + V_{PP}^{min} \qquad (4)$$

where V_{PP}^{max} and V_{PP}^{min} are the maximum and minimum values of the applied peak-to-peak voltage and $n = 1, 2$ is the number of symmetric lobes in $\mathbf{v}(\phi)$. For $n = 1$, the dumbbell velocity is maximal when the particle is aligned with the y axis and minimal when it is aligned with the x axis. In the case of $n = 2$, the dumbbell velocity is maximal for an orientation angle $\pi/4$ and minimal when the particle is aligned with the x or y axis.

There is an inherent delay in capturing an image, extracting the dumbbell angle, and updating the voltage according to it. In our experimental setup, a full cycle takes 400 ms, leading to an update frequency of the particle velocity of 2.5 Hz. This frequency is much lower than the one used to randomize the dumbbell orientation (1

kHz) so that there is a clear separation of time scales between the two types of updates, and the dumbbell undergoes standard rotational diffusion at an imposed rate.

■ RESULTS AND DISCUSSION

Orientation-Dependent Motility. Our active colloidal dumbbells are produced by sequential capillary assembly,[51] as represented in Figure 1a in Materials and Methods, and self-
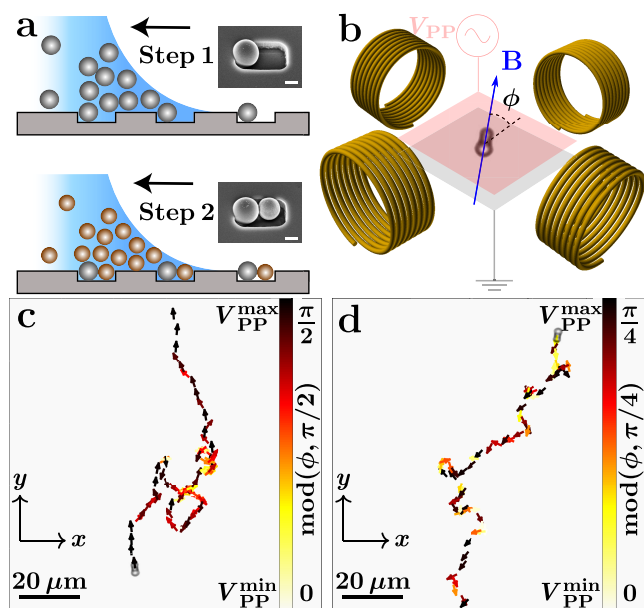
Figure 1. (a) Side-view representation of the sCAPA fabrication of active magnetic dumbbells. The PS particles (gray spheres) are deposited first, followed by the SiO$_2$-mag particles (brown spheres). The black arrows indicate the deposition direction. The insets show SEM images of the particles in the traps after each deposition step (2 μm scale bar). (b) Scheme of the experimental setup. Four magnetic coils impose a randomly oriented magnetic field **B** (blue arrow) to set the rotational diffusivity of the dumbbells to $D_R = 0.25$ rad^2/s. An ac electric field applied between two transparent electrodes is used to actuate the dumbbell with velocity $v \propto V_{PP}^2(t)$. A feedback loop updates the applied voltage as a function of the dumbbell orientation angle $\phi(t)$ to achieve an orientation-dependent propulsion velocity. (c, d) Trajectories of active magnetic dumbbells with a motility with 2-fold (c) and 4-fold (d) rotational symmetry. The particle positions at discrete times are represented by arrows indicating the dumbbell orientation and are color coded according to the applied voltage in the range from V_{PP}^{min} to V_{PP}^{max}, which corresponds to mod($\phi(t), \pi/2$) (c) and mod($\phi(t), \pi/4$) (d). See the corresponding Supporting Information Movies.

propel under an ac electric fields thanks to induced-charge electrophoresis.[56−58] The compositional asymmetry of the dumbbell results in local unbalanced EHD flows producing a net force that generates propulsion along the long axis of the dumbbell.[52,53] In order to achieve robust experimental control of orientational dynamics, we decouple it from the thermal bath by randomizing the dumbbell orientation using an external magnetic field (Figure 1b) to set a constant rotational diffusivity of $D_R = 0.25$ rad^2/s.[54] We furthermore include a feedback loop to update the dumbbell's propulsion velocity according to its orientation, as described in Materials and Methods and sketched in Figure S1 in the Supporting Information, to experimentally realize active Brownian particles with orientation-dependent motility.

In this work, we study two representative orientation-dependent motilities. In the first case, the particle's motility has a 2-fold rotational symmetry, with the lowest velocity occurring when the particle is oriented along the x axis and the highest when it is oriented along the y axis (Figure 1c and Supporting Information Movie 1). We incorporate this motility effectively in leading order as

$$\mathbf{v}_1(\phi) = 2\bar{v}_1 \sin^2 \phi \, \hat{\mathbf{u}}(\phi) \tag{5}$$

where $\bar{v}_1$ denotes the orientationally averaged speed of the particle. In the second case, the velocity has 4-fold symmetry, where the dumbbell achieves the highest velocity when it is aligned along the diagonal corresponding to an orientation angle $\pi/4$ and the lowest when it is aligned with the x or y axis (Figure 1d and Supporting Information Movie 2). This case is analogously described as

$$\mathbf{v}_2(\phi) = 2\bar{v}_2 \sin^2 (2\phi) \, \hat{\mathbf{u}}(\phi) \tag{6}$$

Figure 2 shows that the prescribed motility scenarios are experimentally realized. In Figure 2a,b, we fit eqs 5 and 6 to the
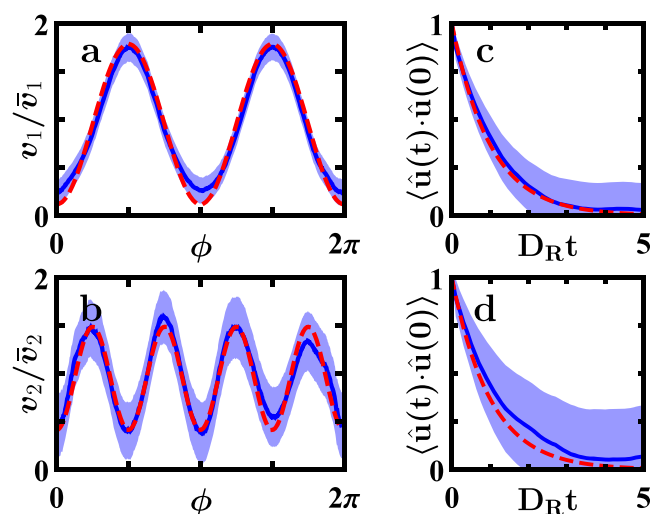
Figure 2. (a, b) Orientation-dependent motility with 2-fold rotational symmetry $v_1(\phi)/\bar{v}_1 = 2 \sin^2 \phi$ and 4-fold rotational symmetry $v_2(\phi)/\bar{v}_2 = 2 \sin^2 (2\phi)$. Solid dark-blue and dashed red curves show the experimental data and a trigonometric fit, respectively. The fits yield $\bar{v}_1 = 1.4$ μm/s and $\bar{v}_2 = 1.1$ μm/s. Light-blue areas express the standard error of the mean. (c, d) Orientation-correlation function $\langle \hat{\mathbf{u}}(t) \cdot \hat{\mathbf{u}}(0) \rangle$ for the two experiments and the expected function $\langle \hat{\mathbf{u}}(t) \cdot \hat{\mathbf{u}}(0) \rangle = \exp(-D_R t)$ for comparison, validating the imposed rotational diffusivity $D_R = 0.25$ rad^2/s.

data for the orientation-dependent velocity observed in the experiments corresponding to the first and second scenario, respectively. We find good agreement of the fit curves and experimental data and determine orientationally averaged speeds $\bar{v}_1 = 1.4$ μm/s and $\bar{v}_2 = 1.1$ μm/s. The orientational decorrelation of the velocity vector obeys a simple exponential decay with a rate corresponding to the imposed rotational diffusivity $D_R = 0.25$ rad^2/s (Figure 2c,d). In the following sections, we will denote all lengths in units of the orientationally averaged persistence length $L = \bar{v}/D_R$ (i.e., $\mathbf{r} \to \mathbf{r}/L$) and time in units of the persistence time $\tau_R = 1/D_R$ (i.e., $t \to D_R t$). The importance of translational noise relative to the imposed speed $\bar{v}$ and rotational diffusion can be defined by the dimensionless Péclet number, $Pe = \bar{v}/\sqrt{D_R D_T}$, where the thermal transla-
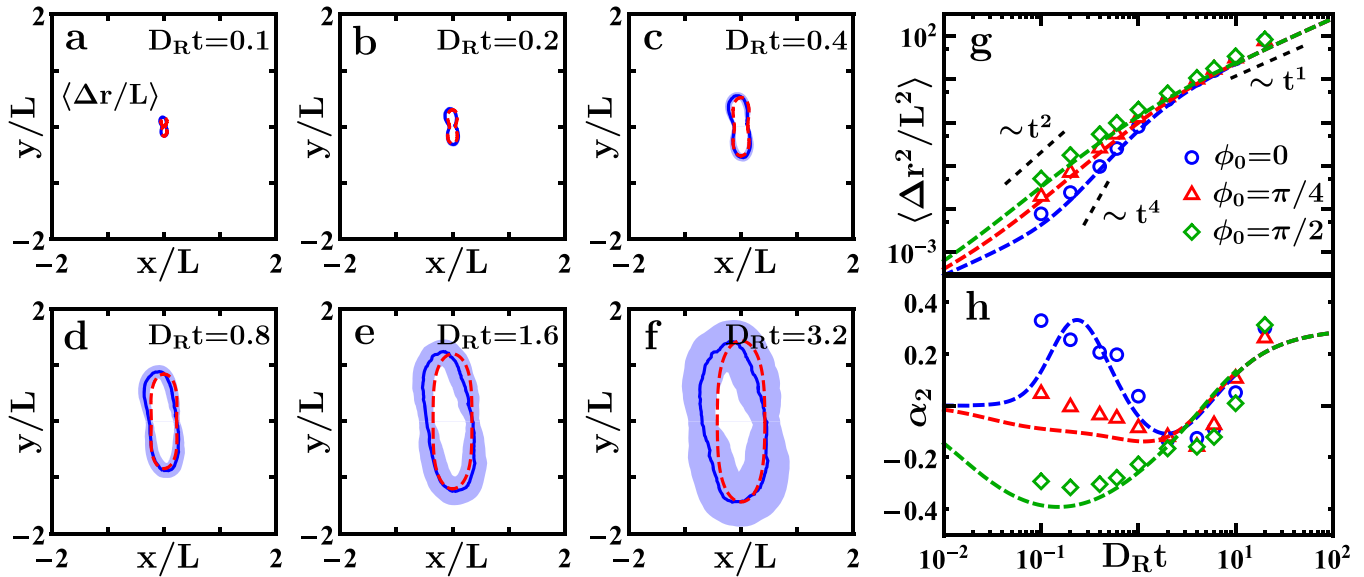
Figure 3. Comparison between theoretical and experimental results for a propulsion velocity with 2-fold symmetry. (a–f) The anisotropic motion of the particle is visualized by plotting the mean displacement $\langle \Delta \mathbf{r}(\phi_0) \rangle$ as a function of the initial orientation ϕ_0 for fixed times (a) $D_R t = 0.1$, (b) $D_R t = 0.2$, (c) $D_R t = 0.4$, (d) $D_R t = 0.8$, (e) $D_R t = 1.6$, and (f) $D_R t = 3.2$. Solid dark-blue and dashed red curves show the experimental data and analytical results, respectively. Light-blue areas express the standard error of the mean. (g) Mean-square displacement $\langle \Delta \mathbf{r}^2(t) \rangle$ for initial orientations $\phi_0 = 0$ (blue), $\phi_0 = \pi/4$ (red), and $\phi_0 = \pi/2$ (green). Symbols and dashed curves show the experimental data and analytical results, respectively. In addition, reference slopes are included for diffusive ($\nu = 1$), ballistic ($\nu = 2$), and quartic ($\nu = 4$) temporal behavior. (h) Non-Gaussian parameter $\alpha_2(t)$ for the same initial orientations. Lengths are given in units of $L = 5.6\ \mu$m and time in units of $1/D_R = 0.4$ s, and the Péclet number is set to $Pe = 12$.

tional diffusion coefficient of the dumbbells was experimentally determined to be $D_T = 0.055\ \mu$m²/s.

Mean Displacement. To characterize the effect of orientation-dependent motility on the Brownian dynamics, we first discuss the mean displacement $\langle \Delta \mathbf{r}(t) \rangle$ of the particle. In Figures 3a–f and 4a–f, the experimentally determined mean displacement is compared with that resulting from our theoretical model, where we emphasize the anisotropic motion of the particle by plotting the mean displacement as a function of the initial orientation $\phi_0 = \phi(0)$ after fixed times t. The theoretical result for the mean displacement is given for a general orientation-dependent motility as

$$\frac{\langle \Delta \mathbf{r}(t) \rangle}{L} = \sum_{\substack{k_1 = -\infty \\ k_1 \neq 0}}^{\infty} \mathbf{c}_{k_1} C_{k_1}(D_R t) e^{ik_1 \phi_0} \tag{7}$$

with

$$C_{k_1}(t) = \frac{1}{k_1^2}(1 - e^{-k_1^2 t}) \tag{8}$$

where the Fourier-coefficient vectors $\mathbf{c}_k$ are determined by the motility $\mathbf{v}(\phi)$. Here, $\mathbf{c}_k = \int_{-\pi}^{\pi} (\mathbf{v}_n(\phi)/(2\pi \bar{v}_n)) \exp(-ik\phi)\, d\phi$ for $n = 1, 2$. (All analytical results for the two studied scenarios are listed explicitly in the Supporting Information.) For short times $t \lesssim \tau_R$, the particle moves linearly in time with $\langle \Delta \mathbf{r}(t) \rangle = \mathbf{v}(\phi_0)t + O(t^2)$, and the anisotropy with respect to the initial orientation, as is visible in Figures 3a and 4a, is a deterministic consequence of the anisotropic propulsion of the particle. For intermediate times $t \approx \tau_R$, the orientation of the particle starts to decorrelate, which directly affects the anisotropic shape of the mean displacement (Figures 3b–e and 4b–e). Finally, for long times $t \gtrsim \tau_R$, the mean displacement saturates to an anisotropic persistence length

$\lim_{t \to \infty} \langle \Delta \mathbf{r}(t) \rangle = L \sum_{k=-\infty, k\neq 0}^{\infty} \mathbf{c}_k e^{ik\phi_0}/k^2$ (Figures 3f and 4f). The faster varying contributions (i.e., the higher Fourier modes) of the propulsion velocity saturate faster and have a smaller impact on the mean motion of the particle, resulting in a more isotropic final shape (cf. Figures 3f and 4).

Mean-Square Displacement. The dynamics of active Brownian motion can be further classified in temporal regimes by investigating the scaling behavior of the mean-square displacement (i.e., $\langle \Delta \mathbf{r}^2(t) \rangle \propto t^\nu$). For $\nu = 1$, the particle shows ordinary diffusive behavior. If $\nu < 1$ or $\nu > 1$, then the particle undergoes subdiffusion or superdiffusion, respectively. The mean-square displacement for a general orientation-dependent motility is given by

$$\frac{\langle \Delta \mathbf{r}^2(t) \rangle}{L^2} = \frac{4 D_R t}{Pe^2} + \sum_{\substack{k_1 = -\infty \\ k_1 \neq 0}}^{\infty} \sum_{\substack{k_2 = -\infty \\ k_2 \neq 0}}^{\infty} \mathbf{c}_{k_1} \cdot \mathbf{c}_{k_2} (C_{k_1 k_2}(D_R t)$$
$$+ C_{k_2 k_1}(D_R t)) e^{i(k_1 + k_2)\phi_0} \tag{9}$$

with

$$C_{k_1 k_2}(t) = $$
$$\begin{cases} \frac{1}{k_2^4}\left(k_2^2 t - (1 - e^{-k_2^2 t})\right), & \text{for } k_1 = -k_2, \\ \frac{1}{k_2^2}\left(1 - (1 + k_2^2 t)e^{-k_2^2 t}\right), & \text{for } k_1 = -2k_2, \\ \frac{1}{k_1(k_1 + 2k_2)}\left(\frac{1}{k_2^2}(1 - e^{-k_1^2 t}) - \frac{1}{(k_1 + k_2)^2}(1 - e^{-(k_1+k_2)^2 t})\right), & \text{else} \end{cases} \tag{10}$$

In Figures 3h and 4h, we compare the experimentally determined mean-square displacement with the corresponding theoretical result. We observe three temporal regimes, characterized by two crossover times. By expanding the
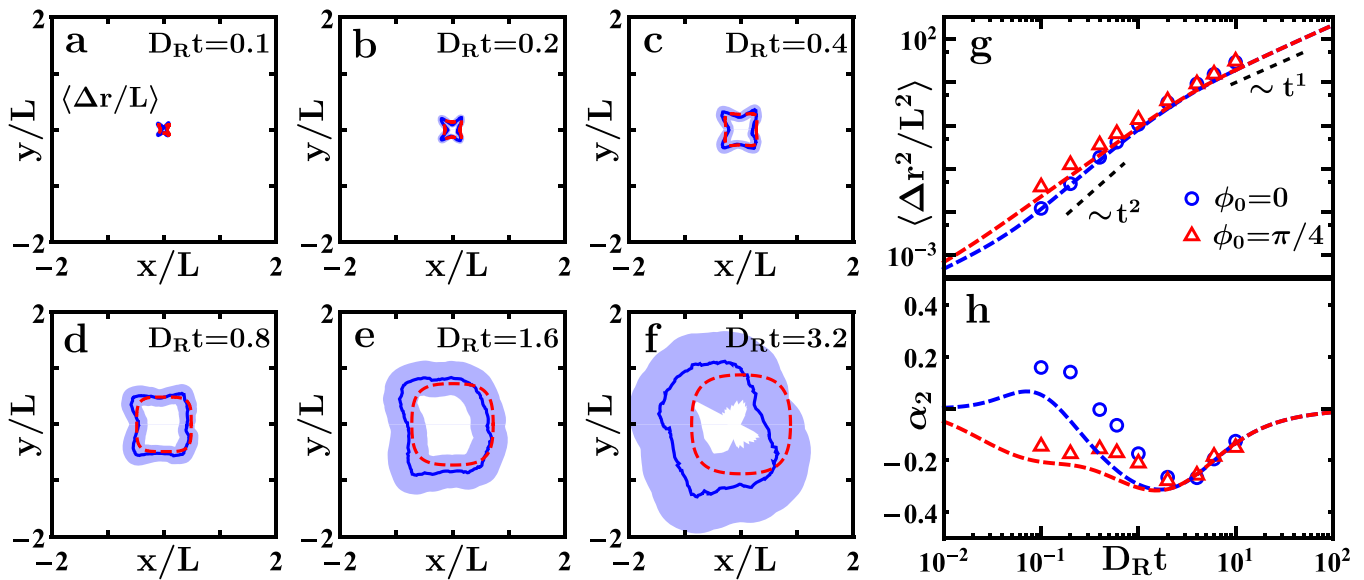
Figure 4. The same as in Figure 3 for a propulsion velocity with 4-fold symmetry. Lengths are given in units of $L = 4.4 \ \mu m$ and time in units of $1/D_R = 0.4$ s, and the Péclet number is $Pe = 9$.

analytical result for the mean-square displacement in time, we obtain

$$\langle \Delta \mathbf{r}^2(t) \rangle = 4 D_T t + \mathbf{v}^2(\phi_0) t^2 + D_R (3 \partial_{\phi_0}^2 \mathbf{v}^2(\phi_0)$$

$$- 2 (\partial_{\phi_0} \mathbf{v}(\phi_0))^2) \frac{t^3}{6} + O(t^4) \tag{11}$$

where ∂_{ϕ_0} denotes the partial derivative with respect to the initial orientation ϕ_0. Thus, the mean-square displacement starts in a short-time diffusion regime ($\nu = 1$), increasing linearly in time with the short-time diffusion coefficient $D_S = D_T$. A transition from the short-time diffusive regime to a superdiffusive regime ($\nu > 1$) occurs if the deterministic swimming motion dominates translational diffusion. This condition is fulfilled for times t greater than the translational diffusion time $\tau_D = D_T / \mathbf{v}^2(\phi_0)$. As shown in Figure 3h, the transition to an intermediate superdiffusive regime is sensitive with respect to the initial velocity. If the particle is oriented initially along directions of high motility (see Figure 3h for $\phi_0 = \pi/2$), then the mean-square displacement displays a crossover to the ballistic regime ($\nu = 2$). However, if the initial velocity of the particle is not large enough to dominate translational diffusion or even vanishes (eq 11), then we observe a delayed crossover (see Figure 3h for $\phi_0 = 0$). In that case, the particle has to undergo an angular displacement first such that its propulsion grows until it overcomes translational diffusion. Due to this multiplicative coupling of diffusive and ballistic behavior for the angular and positional displacements, respectively, the mean-square displacement shows a superballistic power-law behavior ($\nu > 2$), which is masked by finite translational diffusion (eq 11). For the specific initial orientation $\phi_0 = 0$, the second- and even third-order terms in eq 11 vanish such that the next leading order after normal diffusion scales even quartically ($\nu = 4$), which is more visible for a higher Péclet number Pe. (See Figure S2 in the Supporting Information for the emergence of this scaling regime.) For times t greater than the rotational diffusion time $\tau_R = 1/D_R$, the mean-square displacement evolves toward the diffusive limit ($\nu = 1$) again, and it is described by a long-time diffusion coefficient

$$D_L = \lim_{t \to \infty} \frac{\langle \Delta \mathbf{r}^2(t) \rangle}{4t} = D_T + \frac{\bar{v}^2}{D_R} \sum_{k_1 = 1}^{\infty} \frac{|c_{k_1}|^2}{k_1^2} \tag{12}$$

In the two experimental scenarios, the long-time diffusion coefficients are $D_{L,1} = 5.1 \ \mu m^2/s$ and $D_{L,2} = 2.6 \ \mu m^2/s$, respectively.

Non-Gaussian Parameter. Finally, we study the non-Gaussian features of our active dynamics in more detail. Hence, we introduce the non-Gaussian parameter, which is defined in two spatial dimensions as[59]

$$\alpha_2(t) = \frac{1}{2} \frac{\langle \Delta \mathbf{r}^4(t) \rangle}{\langle \Delta \mathbf{r}^2(t) \rangle^2} - 1 \tag{13}$$

The non-Gaussian parameter quantifies how far the distribution of displacements deviates from a Gaussian (i.e., $\alpha_2(t) = 0$ for an isotropic Gaussian distribution). For $\alpha_2(t) < 0$ or $\alpha_2(t) > 0$, the underlying distribution has less- or more-pronounced tails, respectively. Interesting for active Brownian motion is the case of deterministic motion (no tails), for which the non-Gaussian parameter is $\alpha_2(t) = -1/2$. To derive the analytical expression for the non-Gaussian parameter from our theoretical model, in addition to the mean-square displacement $\langle \Delta \mathbf{r}^2(t) \rangle$ the mean-quartic displacement $\langle \Delta \mathbf{r}^4(t) \rangle$ is also required, which is explicitly calculated in the Supporting Information. In Figures 3h and 4h, the anisotropy of the non-Gaussian behavior is visualized. For very small times $t \ll \tau_D$, the displacements are simply diffusive (i.e., Gaussian), thus the non-Gaussian parameter $\alpha_2(t)$ is zero. For intermediate times $\tau_D < t < \tau_R$, the non-Gaussian parameter behaves anisotropically with respect to the initial orientation ϕ_0. For a sufficiently high initial velocity, $\alpha_2(t)$ becomes negative, which is characteristic of persistently swimming Brownian particles (see Figure 3h for $\phi_0 = \pi/2$). When the initial velocity vanishes (i.e., $\mathbf{v}(\phi_0) = 0$; see Figure 3h for $\phi_0 = 0$), we observe a positive non-Gaussian parameter. In this case, the particle moves mostly diffusively even for intermediate times, except for rare events where a fluctuation rotates the particle sufficiently such that it experiences a large ballistic step. The underlying distribution of displacements is thus Gaussian with pronounced tails which

dominate the fourth moment over the second and lead to positive non-Gaussian character. Finally, for long times $t > \tau_R$, we observe long-lived non-Gaussian behavior in the case of 2-fold symmetry and Gaussian behavior in the case of 4-fold symmetry. To explain this observation, we consider the covariance matrix of the displacement distribution, and we define the long-time diffusion matrix

$$
\begin{aligned}
(\mathbf{D}_L)_{ij} &= \lim_{t \to \infty} \frac{\langle \Delta r_i(t)\, \Delta r_j(t) \rangle}{2t} \\
&= D_T \delta_{ij} + \frac{\bar{v}^2}{D_R} \sum_{k_1=1}^{\infty} \frac{1}{k_1^2} (c_{k_1,i} c_{-k_1,j} + c_{-k_1,i} c_{k_1,j})
\end{aligned}
\tag{14}
$$

for $i, j \in \{x, y\}$. The eigenvalues of this matrix are given as $D_\pm = D_L \pm \Delta D_L$, where ΔD_L denotes the long-time anisotropy

$$
\Delta D_L = \frac{\bar{v}^2}{D_R} \sqrt{\sum_{k_1=1}^{\infty} \sum_{k_2=1}^{\infty} \frac{1}{k_1^2 k_2^2} (|\mathbf{c}_{k_1} \cdot \mathbf{c}_{k_2}|^2 + |\mathbf{c}_{k_1} \cdot \mathbf{c}_{-k_2}|^2 - |\mathbf{c}_{k_1}|^2 |\mathbf{c}_{k_2}|^2)}
\tag{15}
$$

which describes the long-time diffusion along the principal axes of maximal and minimal diffusion, respectively. In the two experimental scenarios, the long-time anisotropy yields $\Delta D_{L,1} = 4.0\ \mu m^2/s$ and $\Delta D_{L,2} = 0\ \mu m^2/s$, respectively. Using the introduced notation, the long-time behavior of the non-Gaussian parameter can be expressed as

$$
\lim_{t \to \infty} \alpha_2(t) = \frac{1}{2} \left(\frac{\Delta D_L}{D_L} \right)^2
\tag{16}
$$

which coincides with the non-Gaussian character of an anisotropic Gaussian distribution with covariance matrix $2\mathbf{D}_L t$. Thus, the long-time behavior of the non-Gaussian parameter quantifies the anisotropy of the long-time diffusion. For the motility with 2-fold symmetry, we have enhanced long-time diffusion along the y axis and decreased long-time diffusion along the x axis leading to non-Gaussian character for long times (Figure 3h). In the second scenario, the long-time behavior can be described with solely one long-time diffusion coefficient, thus the non-Gaussian parameter vanishes (Figure 4h).

CONCLUSIONS

In this work, we reported on a new methodology to impose complex anisotropic motility behavior on active Brownian particles. We engineered the orientation-dependent motility of active dumbbells whose rotational diffusivity is externally controlled by randomized magnetic fields and whose propulsion velocity is prescribed using a feedback scheme, which updates the velocity based on the particles' orientation. To describe the dynamic features of the particles, we developed a theoretical framework that proved to be in good agreement with the corresponding experimental data. In particular, a particle's mean displacement shows deterministic active motion at very short times, decorrelation at intermediate times, and saturation to anisotropic persistence trajectories at long times. The mean-square displacement is also characterized by different temporal regimes. We found that the transition from isotropic diffusion at short times to a superdiffusive intermediate regime is very sensitive to the initial velocity of the particle such that the coupling of diffusive-rotational and ballistic-translational motion can result in superballistic motion. Moreover, the motion is characterized by anisotropic diffusion at long times, as described by the long-time diffusion coefficient and the long-time anisotropy. Finally, we have investigated the deviation from a

standard Gaussian distribution by calculating the non-Gaussian parameter as a function of time. It becomes nonzero for intermediate times: negative when there is persistent swimming and positive during reorientation events from an initial orientation with low velocity to orientations with high velocity. Furthermore, the long-time behavior quantifies the anisotropy of the long-time diffusion, being nonzero for the 2-fold-symmetric motility and zero for the 4-fold-symmetric motility.

The basic model we proposed here is applicable to a broad range of systems with anisotropic external propulsion mechanisms and relevant in the context of the orientational dependence of the propulsion speed, which can intrinsically emerge for both artificial and biological microswimmers.[50,55] In the future, intricate combinations of spatial, orientational, and temporal modulations of motility could be considered. One could also proceed to particles with a complex shape, which have more involved trajectories.[60,61] Finally, although in our current experiments one particle at a time is controlled, we envision possible experimental realizations to control many particles to explore emerging collective effects.[62]

ASSOCIATED CONTENT

ⓢ Supporting Information

The Supporting Information is available free of charge at https://pubs.acs.org/doi/10.1021/acs.langmuir.9b03617.

> Real-time feedback applied in the experiments; details of the postprocessing and data analysis; expressions for the nth moment of the translational displacement $\langle \Delta \mathbf{r}^n(t) \rangle$ for active Brownian motion with a general orientation-dependent motility; expressions for the low-order moments corresponding to the two studied motility scenarios; the emergence of the quartic intermediate regime for a propulsion velocity with 2-fold symmetry and a large Péclet number (PDF)

> Representative trajectory of a dumbbell with a motility with 2-fold symmetry (AVI)

> Representative trajectory of a dumbbell with a motility with 4-fold symmetry (AVI)

AUTHOR INFORMATION

Corresponding Authors

    Lucio Isa − *Laboratory for Soft Materials and Interfaces, Department of Materials, ETH Zürich, 8093 Zürich, Switzerland;* ⓘ orcid.org/0000-0001-6731-9620; Email: lucio.isa@mat.ethz.ch

    Raphael Wittkowski − *Institut für Theoretische Physik, Center for Soft Nanoscience, Westfälische Wilhelms-Universität Münster, D-48149 Münster, Germany;* ⓘ orcid.org/0000-0003-4881-9173; Email: raphael.wittkowski@uni-muenster.de

Authors

    Alexander R. Sprenger − *Institut für Theoretische Physik II: Weiche Materie, Heinrich-Heine-Universität Düsseldorf, D-40225 Düsseldorf, Germany*

    Miguel Angel Fernandez-Rodriguez − *Laboratory for Soft Materials and Interfaces, Department of Materials, ETH Zürich, 8093 Zürich, Switzerland*

    Laura Alvarez − *Laboratory for Soft Materials and Interfaces, Department of Materials, ETH Zürich, 8093 Zürich, Switzerland;* ⓘ orcid.org/0000-0001-7018-7817

Hartmut Löwen − *Institut für Theoretische Physik II: Weiche Materie, Heinrich-Heine-Universität Düsseldorf, D-40225 Düsseldorf, Germany*

Complete contact information is available at:
https://pubs.acs.org/10.1021/acs.langmuir.9b03617

Notes

■ ACKNOWLEDGMENTS

■ REFERENCES

(1) Bechinger, C.; Di Leonardo, R.; Löwen, H.; Reichhardt, C.; Volpe, G.; Volpe, G. Active particles in complex and crowded environments. *Rev. Mod. Phys.* **2016**, *88*, No. 045006.

(2) Ebbens, S. J.; Howse, J. R. In pursuit of propulsion at the nanoscale. *Soft Matter* **2010**, *6*, 726−738.

(3) Romanczuk, P.; Bär, M.; Ebeling, W.; Lindner, B.; Schimansky-Geier, L. Active Brownian particles. From individual to collective stochastic dynamics. *Eur. Phys. J.: Spec. Top.* **2012**, *202*, 1−162.

(4) Elgeti, J.; Winkler, R. G.; Gompper, G. Physics of microswimmers−single particle motion and collective behavior: a review. *Rep. Prog. Phys.* **2015**, *78*, No. 056601.

(5) Zöttl, A.; Stark, H. Emergent behavior in active colloids. *J. Phys.: Condens. Matter* **2016**, *28*, No. 253001.

(6) Paxton, W. F.; Kistler, K. C.; Olmeda, C. C.; Sen, A.; St. Angelo, S. K.; Cao, Y.; Mallouk, T. E.; Lammert, P. E.; Crespi, V. H. Catalytic nanomotors: autonomous movement of striped nanorods. *J. Am. Chem. Soc.* **2004**, *126*, 13424−13431.

(7) Palacci, J.; Cottin-Bizonne, C.; Ybert, C.; Bocquet, L. Sedimentation and effective temperature of active colloidal suspensions. *Phys. Rev. Lett.* **2010**, *105*, No. 088304.

(8) Dietrich, K.; Renggli, D.; Zanini, M.; Volpe, G.; Buttinoni, I.; Isa, L. Two-dimensional nature of the active Brownian motion of catalytic microswimmers at solid and liquid interfaces. *New J. Phys.* **2017**, *19*, No. 065008.

(9) Volpe, G.; Buttinoni, I.; Vogt, D.; Kümmerer, H.-J.; Bechinger, C. Microswimmers in patterned environments. *Soft Matter* **2011**, *7*, 8810−8815.

(10) Buttinoni, I.; Volpe, G.; Kümmel, F.; Volpe, G.; Bechinger, C. Active Brownian motion tunable by light. *J. Phys.: Condens. Matter* **2012**, *24*, No. 284129.

(11) Palacci, J.; Sacanna, S.; Steinberg, A.; Pine, D.; Chaikin, P. Living crystals of lightactivated colloidal surfers. *Science* **2013**, *339*, 936−940.

(12) Palacci, J.; Sacanna, S.; Vatchinsky, A.; Chaikin, P. M.; Pine, D. J. Photoactivated colloidal dockers for cargo transportation. *J. Am. Chem. Soc.* **2013**, *135*, 15978−15981.

(13) Palacci, J.; Sacanna, S.; Kim, S.-H.; Yi, G.-R.; Pine, D. J.; Chaikin, P. M. Lightactivated self-propelled colloids. *Philos. Trans. R. Soc., A* **2014**, *372*, No. 20130372.

(14) Moyses, H.; Palacci, J.; Sacanna, S.; Grier, D. G. Trochoidal trajectories of self-propelled Janus particles in a diverging laser beam. *Soft Matter* **2016**, *12*, 6357−6364.

(15) Wang, W.; Castro, L. A.; Hoyos, M.; Mallouk, T. E. Autonomous motion of metallic microrods propelled by ultrasound. *ACS Nano* **2012**, *6*, 6122−6132.

(16) Dreyfus, R.; Baudry, J.; Roper, M. L.; Fermigier, M.; Stone, H. A.; Bibette, J. Microscopic artificial swimmers. *Nature* **2005**, *437*, 862−865.

(17) Grosjean, G.; Lagubeau, G.; Darras, A.; Hubert, M.; Lumay, G.; Vandewalle, N. Remote control of self-assembled microswimmers. *Sci. Rep.* **2015**, *5*, No. 16035.

(18) Steinbach, G.; Gemming, S.; Erbe, A. Non-equilibrium dynamics of magnetically anisotropic particles under oscillating fields. *Eur. Phys. J. E: Soft Matter Biol. Phys.* **2016**, *39*, No. 69.

(19) Kaiser, A.; Snezhko, A.; Aranson, I. S. Flocking ferromagnetic colloids. *Science Advances* **2017**, *3*, No. e1601469.

(20) Bricard, A.; Caussin, J. B.; Desreumaux, N.; Dauchot, O.; Bartolo, D. Emergence of macroscopic directed motion in populations of motile colloids. *Nature* **2013**, *503*, 95−98.

(21) Morin, A.; Desreumaux, N.; Caussin, J.-B.; Bartolo, D. Distortion and destruction of colloidal flocks in disordered environments. *Nat. Phys.* **2017**, *13*, 63−67.

(22) Kümmel, F.; ten Hagen, B.; Wittkowski, R.; Buttinoni, I.; Eichhorn, R.; Volpe, G.; Löwen, H.; Bechinger, C. Circular motion of asymmetric self-propelling particles. *Phys. Rev. Lett.* **2013**, *110*, No. 198302.

(23) Kümmel, F.; ten Hagen, B.; Wittkowski, R.; Takagi, D.; Buttinoni, I.; Eichhorn, R.; Volpe, G.; Löwen, H.; Bechinger, C. Reply to "Comment on 'Circular motion of asymmetric self-propelling particles'. *Phys. Rev. Lett.* **2014**, *113*, No. 029802.

(24) Zheng, X.; ten Hagen, B.; Kaiser, A.; Wu, M.; Cui, H.; Silber-Li, Z.; Löwen, H. Non-Gaussian statistics for the motion of self-propelled Janus particles: experiment versus theory. *Phys. Rev. E* **2013**, *88*, No. 032304.

(25) Hong, Y.; Blackman, N. M.; Kopp, N. D.; Sen, A.; Velegol, D. Chemotaxis of nonbiological colloidal rods. *Phys. Rev. Lett.* **2007**, *99*, No. 178103.

(26) Pohl, O.; Stark, H. Dynamic clustering and chemotactic collapse of self-phoretic active particles. *Phys. Rev. Lett.* **2014**, *112*, No. 238303.

(27) Saha, S.; Golestanian, R.; Ramaswamy, S. Clusters, asters, and collective oscillations in chemotactic colloids. *Phys. Rev. E* **2014**, *89*, No. 062316.

(28) Liebchen, B.; Marenduzzo, D.; Pagonabarraga, I.; Cates, M. E. Clustering and pattern formation in chemorepulsive active colloids. *Phys. Rev. Lett.* **2015**, *115*, No. 258301.

(29) Liebchen, B.; Marenduzzo, D.; Cates, M. E. Phoretic interactions generically induce dynamic clusters and wave patterns in active colloids. *Phys. Rev. Lett.* **2017**, *118*, No. 268001.

(30) Jin, C.; Krüger, C.; Maass, C. C. Chemotaxis and autochemotaxis of self-propelling droplet swimmers. *Proc. Natl. Acad. Sci. U. S. A.* **2017**, *114*, 5089−5094.

(31) Lozano, C.; ten Hagen, B.; Löwen, H.; Bechinger, C. Phototaxis of synthetic microswimmers in optical landscapes. *Nat. Commun.* **2016**, *7*, No.12828.

(32) Garcia, X.; Rafaï, S.; Peyla, P. Light control of the flow of phototactic microswimmer suspensions. *Phys. Rev. Lett.* **2013**, *110*, No. 138106.

(33) Geiseler, A.; Hänggi, P.; Marchesoni, F.; Mulhern, C.; Savel'ev, S. Chemotaxis of artificial microswimmers in active density waves. *Phys. Rev. E: Stat. Phys., Plasmas, Fluids, Relat. Interdiscip. Top.* **2016**, *94*, No. 012613.

(34) Geiseler, A.; Hänggi, P.; Marchesoni, F. Self-polarizing microswimmers in active density waves. *Sci. Rep.* **2017**, *7*, No. 41884.

(35) Geiseler, A.; Hänggi, P.; Marchesoni, F. Taxis of artificial swimmers in a spatiotemporally modulated activation medium. *Entropy* **2017**, *19*, No. 97.

(36) Sharma, A.; Brader, J. M. Brownian systems with spatially inhomogeneous activity. *Phys. Rev. E: Stat. Phys., Plasmas, Fluids, Relat. Interdiscip. Top.* **2017**, *96*, No. 032604.

(37) Dai, B.; Wang, J.; Xiong, Z.; Zhan, X.; Dai, W.; Li, C.-C.; Feng, S.-P.; Tang, J. Programmable artificial phototactic microswimmer. *Nat. Nanotechnol.* **2016**, *11*, 1087−1092.

(38) Li, W.; Wu, X.; Qin, H.; Zhao, Z.; Liu, H. Light-driven and light-guided microswimmers. *Adv. Funct. Mater.* **2016**, *26*, 3164−3171.

(39) Lozano, C.; Bechinger, C. Diffusing wave paradox of phototactic particles in traveling light pulses. *Nat. Commun.* **2019**, *10*, No. 2495.

(40) Lozano, C.; Liebchen, B.; ten Hagen, B.; Bechinger, C.; Löwen, H. Propagating density spikes in light-powered motility-ratchets. *Soft Matter* **2019**, *15*, 5185−5192.

(41) Palagi, S.; Singh, D. P.; Fischer, P. Light-controlled micromotors and soft microrobots. *Adv. Opt. Mater.* **2019**, *7*, No. 1900370.

(42) Ghosh, P. K.; Li, Y.; Marchesoni, F.; Nori, F. Pseudochemotactic drifts of artificial microswimmers. *Phys. Rev. E* **2015**, *92*, No. 012114.

(43) Magiera, M. P.; Brendel, L. Trapping of interacting propelled colloidal particles in inhomogeneous media. *Phys. Rev. E* **2015**, *92*, No. 012304.

(44) Grauer, J.; Löwen, H.; Janssen, L. M. C. Spontaneous membrane formation and self-encapsulation of active rods in an inhomogeneous motility field. *Phys. Rev. E: Stat. Phys., Plasmas, Fluids, Relat. Interdiscip. Top.* **2018**, *97*, No. 022608.

(45) Scacchi, A.; Brader, J. M.; Sharma, A. Escape rate of transiently active Brownian particle in one dimension. *Phys. Rev. E: Stat. Phys., Plasmas, Fluids, Relat. Interdiscip. Top.* **2019**, *100*, No. 012601.

(46) Vuijk, H. D.; Brader, J. M.; Sharma, A. Anomalous fluxes in overdamped Brownian dynamics with Lorentz force. *J. Stat. Mech.: Theory Exp.* **2019**, *2019*, No. 063203.

(47) Merlitz, H.; Vuijk, H. D.; Brader, J.; Sharma, A.; Sommer, J.-U. Linear response approach to active Brownian particles in time-varying activity fields. *J. Chem. Phys.* **2018**, *148*, No. 194116.

(48) Liebchen, B.; Löwen, H. Optimal navigation strategies for active particles. *EPL* **2019**, *127*, No.34003.

(49) Maggi, C.; Angelani, L.; Frangipane, G.; Di Leonardo, R. Currents and flux-inversion in photokinetic active particles. *Soft Matter* **2018**, *14*, 4958−4962.

(50) Uspal, W. E. Theory of light-activated catalytic Janus particles. *J. Chem. Phys.* **2019**, *150*, No. 114903.

(51) Ni, S.; Leemann, J.; Buttinoni, I.; Isa, L.; Wolf, H. Programmable colloidal molecules from sequential capillarity-assisted particle assembly. *Science Advances* **2016**, *2*, No. e1501779.

(52) Ma, F.; Yang, X.; Zhao, H.; Wu, N. Inducing propulsion of colloidal dimers by breaking the symmetry in electrohydrodynamic flow. *Phys. Rev. Lett.* **2015**, *115*, No. 208302.

(53) Ni, S.; Marini, E.; Buttinoni, I.; Wolf, H.; Isa, L. Hybrid colloidal microswimmers through sequential capillary assembly. *Soft Matter* **2017**, *13*, 4252−4259.

(54) Fernandez-Rodriguez, M. A.; Grillo, F.; Alvarez, L.; Rathlef, M.; Buttinoni, I.; Volpe, G.; Isa, L. Active colloids with position-dependent rotational diffusivity. *arXiv:1911.02291*, 2019.

(55) Hu, J.; Wysocki, A.; Winkler, R. G.; Gompper, G. Physical sensing of surface properties by microswimmers − directing bacterial motion via wall slip. *Sci. Rep.* **2015**, *5*, No. 9586.

(56) Squires, T. M.; Bazant, M. Z. Breaking symmetries in induced-charge electro-osmosis and electrophoresis. *J. Fluid Mech.* **2006**, *560*, 65−101.

(57) Gangwal, S.; Cayre, O. J.; Bazant, M. Z.; Velev, O. D. Induced-Charge Electrophoresis of Metallodielectric Particles. *Phys. Rev. Lett.* **2008**, *100*, No. 058302.

(58) Yan, J.; Han, M.; Zhang, J.; Xu, C.; Luijten, E.; Granick, S. Reconfiguring active particles by electrostatic imbalance. *Nat. Mater.* **2016**, *15*, 1095−1099.

(59) Kurzthaler, C.; Franosch, T. Intermediate scattering function of an anisotropic Brownian circle swimmer. *Soft Matter* **2017**, *13*, 6396−6406.

(60) Wittkowski, R.; Löwen, H. Self-propelled Brownian spinning top: dynamics of a biaxial swimmer at low Reynolds numbers. *Phys. Rev. E* **2012**, *85*, No. 021406.

(61) Voß, J.; Wittkowski, R. Hydrodynamic resistance matrices of colloidal particles with various shapes. *arXiv:1811.01269*, 2018.

(62) Cohen, J. A.; Golestanian, R. Emergent cometlike swarming of optically driven thermally active colloids. *Phys. Rev. Lett.* **2014**, *112*, No. 068302.

■ NOTE ADDED AFTER ASAP PUBLICATION

Due to a production oversight, this article was published February 12, 2020 with several formatting issues. The corrected article was published February 17, 2020.